Modular mechanism of Wnt signaling inhibition by Wnt inhibitory factor 1

Tomas Malinauskas, A. Radu Aricescu, Weixian Lu, Christian Siebold &

E. Yvonne Jones

Division of Structural Biology, Wellcome Trust Centre for Human Genetics,

University of Oxford, Oxford, OX3 7BN, UK

Correspondence should be addressed to C.S. (christian@strubi.ox.ac.uk) or E.Y.J.

(yvonne@strubi.ox.ac.uk)

Supplementary Information

This PDF file includes:

Supplementary Methods

Supplementary Figures 1 to 9

Supplementary References

SUPPLEMENTARY METHODS

Crystallization and data collection. Proteins were concentrated by ultrafiltration prior to crystallization: WIF-1_{WD} (9.2 mg ml^{-1}), WIF-$1_{WD\text{-}EGF\text{-}I}$ (7.8 mg ml^{-1}), WIF-$1_{WD\text{-}EGF\text{-}I}$ Met77Trp (10.3 mg ml^{-1}), WIF-$1_{\Delta C}$ (6.5 mg ml^{-1}). Crystals were grown at 21 °C using the sitting drop vapor diffusion method with 100 nl protein plus 100 nl reservoir solution[1]. WIF-1_{WD} crystallized in PEG 8000 30 % w/v, 200 mM sodium acetate, 100 mM sodium cacodylate pH 6.5; WIF-$1_{WD\text{-}EGF\text{-}I}$ in 1.3 M diammonium tartrate, 100 mM bis-tris propane pH 7.0; WIF-$1_{WD\text{-}EGF\text{-}I}$ Met77Trp in 1.1 M diammonium tartrate pH 7.0, 20 mM spermidine, 0.5 mM $CaCl_2$; WIF-$1_{\Delta C}$ in 0.75 M sodium succinate pH 5.7, 35 mg ml^{-1} sucrose octasulfate. Crystals were flash frozen by immersion of the crystal into a reservoir solution containing 25 % (WIF-$1_{\Delta C}$) or 30 % v/v (WIF-1_{WD}, WIF-$1_{WD\text{-}EGF\text{-}I}$, WIF-$1_{WD\text{-}EGF\text{-}I}$ Met77Trp) glycerol followed by transfer to liquid nitrogen. The crystals were kept at 100 K during X-ray diffraction data collection. Diffraction data were processed and scaled with the HKL-2000 program package[2] (except WIF-$1_{WD\text{-}EGF\text{-}I}$ Met77Trp data that were processed and scaled with XDS[3] and SCALA[4]). Data collection statistics are shown in **Table 1**.

Structure determination and refinement. The crystal structure of WIF-1_{WD} was solved by molecular replacement using the WD coordinates determined by NMR spectroscopy[5] as search model in the program Phaser[6]. The initial electron density maps of the WD (immediately after molecular replacement) revealed the architecture of a hydrophobic pocket which appeared to be occupied by lipid-like ligand. A selection of different phosphatidyl cholines were identified as the WIF-1 lipid ligands by mass

spectrometry. DPPC was built into the electron density and included in the model for refinement. The crystal structure of WIF-$1_{WD\text{-}EGF\text{-}I}$ was phased by molecular replacement in Phaser using the WIF-1_{WD} structure (with DPPC omitted) and DPPC was again built into the electron density. Structures were refined using iterative cycles of Coot[7], autoBUSTER[8], and Phenix software suite[9]. The WIF-$1_{WD\text{-}EGF\text{-}I}$ structure also reveals a potential metal-binding site. Based on coordination geometry, a sodium ion was built, which is coordinated by three water molecules (distance 2.5-2.8 Å) and the two protein backbone oxygens of Cys186 (distance 2.3 Å) and Gly190 (distance 2.5 Å)[10]. The composite omit electron density map[11] (**Fig. 1c**) was calculated using Phenix[9].

Initial phases for the WIF-$1_{\Delta C}$ X-ray diffraction data were determined by molecular replacement using the high resolution crystal structure of WIF-1 WD as the search model in Phaser. Phases were improved by solvent flattening and histogram matching using the program Parrot[12]. The resulting electron density map was sufficiently clear to place models of the first three EGF-like domains (**Supplementary Fig. 9**). Structure refinement iterated cycles of restrained refinement in autoBUSTER[8], Phenix[9] and manual rebuilding with Coot[7]. No interpretable density was found for EGFs IV-V; these domains are accommodated within solvent channels and appear to retain significant flexibility within the crystal. All structures have been validated with MolProbity[13].

Mass spectrometry analysis of WIF-1-bound lipids. WIF-1-bound lipids were extracted into $CHCl_3$ plus CH_3OH (2:1 ratio, v/v) at 65 °C, 30 min. The $CHCl_3$ plus CH_3OH-lipid fraction was washed with water three times and concentrated by

evaporation at room temperature. The sample was analyzed by matrix assisted laser desorption ionization time-of-flight mass spectrometry (MALDI-TOF-MS) on a Bruker Daltonics Ultraflex TOF/TOF mass spectrometer. The sample solution was premixed with the matrix (20 mg ml^{-1} 2,5-dihydroxybenzoic acid in 0.1 % v/v trifluoroacetic acid, 30 % v/v acetonitrile) at a 1:1 ratio and 1 µl of mixture applied directly to the sample plate. The droplet was air-dried before analysis in the mass spectrometer. All positive mode MALDI-TOF-MS spectra were obtained in reflection mode. The ionization source was a nitrogen laser, emitting 337 nm electromagnetic radiation in 3-ns pulse. The accelerating voltage in the ion source was 30 kV. Peaks of phosphatidylcholines in the MALDI-TOF mass spectrum (**Fig. 1e**) were assigned according to Schiller et al.[14].

WIF-$1_{\Delta C}$ - lipid interactions. Purified WIF-$1_{\Delta C}$ (270 µl, final conc. 50 µM) was incubated with 16:0 Liss Rhod PE (1,2-dipalmitoyl-*sn*-glycero-3-phosphoethanolamine-N-(lissamine rhodamine B sulfonyl) ammonium salt, 10 µl of 1 mg ml^{-1} Liss Rhod PE in $CHCl_3$, Avanti Polar Lipids) or sulforhodamine B (final conc. 160 µM, Sigma-Aldrich) in PBS (10 mM sodium/potassium phosphate, 2.7 mM KCl and 137 mM NaCl, pH 7.4, at 25 °C, Sigma), 1 % w/v CHAPS for 3 h at 37 °C. To remove the excess of 16:0 Liss Rhod PE, the sample was loaded onto a pre-equilibrated Superdex 200 10/300 column (GE Healthcare Life Sciences) after incubation and gel filtration was performed in PBS, 1 % w/v CHAPS at a flow rate 0.4 ml min^{-1}; WIF-$1_{\Delta C}$ peak fractions were pooled and gel filtration was performed again in PBS without CHAPS. Protein and fluorescent molecule elution was followed by absorption at 280, 557 and 571 nm simultaneously. The fluorescence intensity (excitation at 535 nm, emission at 595 nm) was measured on the Infinite F200 (Tecan) microplate reader. Experiments

with membrane lipid strips (Echelon Biosciences) were performed according to manufacturer's instructions. Proteins on the strips were visualized by Western blotting and chemiluminescence using the Amersham ECL detection kit (GE Healthcare Life Sciences) (**Supplementary Fig. 5**).

Cellular assays for Wnt signaling. HEK293T cells were maintained in DMEM (Sigma) supplemented with L-Gln, non-essential amino acids (Gibco) and 10 % v/v foetal calf serum (FCS, Sigma) in a humidified 37 °C incubator with 5 % v/v CO_2. Cells were seeded in 6-well plates (Corning), ~2×10^6 cells per well and allowed to recover overnight. The cells were then transfected with Super-TOPFlash plasmid[15] (10 µg per well; the plasmid contains 11 TCF/LEF-binding sites upstream of the firefly luciferase gene) using lipofectamine 2000 (10 µg per well, Invitrogen) in media containing 2 % v/v FCS, incubated for 5 h. Then the media was changed to media containing 10 % v/v FCS. Luciferase expression was induced by adding purified human Wnt3a (350 ng per well, equal to 4.7 nM, R&D Systems) into the media. Cells were incubated for 72 h either in the presence or absence of purified WIF-1 constructs or bovine serum albumin (BSA, New England Biolabs) as a control. The cells were washed with PBS buffer, lysed and luciferase activity was measured using the Luciferase Assay System (Promega). The luciferase activity from Super-TOPFlash plasmid transfected cells treated with Wnt3a only was taken as 100 %. The effect of BSA on Wnt3a signaling was below the error level (data not shown). Experiments were performed in triplicate.

SPR binding studies of WIF-1 and Wnt3a. Surface plasmon resonance (SPR)

experiments were performed using a Biacore T100 machine (GE Healthcare) at 25 °C in PBS, 1 % w/v CHAPS buffer. All WIF-1 constructs were purified by SEC in SPR running buffer immediately before use. WIF-1 concentrations were determined from the absorbance at 280 nm using calculated molar extinction coefficients. Purified Wnt3a and streptavidin (control protein, Thermo Fisher Scientific) were immobilized on a CM5 BIAcore sensor chip (Biacore Life Sciences) via primary amines. For measurements of WIF-1 binding to immobilized proteins, samples were injected at 10 µl min^{-1}. The signal from experimental flow cells was corrected by subtraction of a buffer and reference signal from a control protein coupled flow cell. After each injection, the sensor surface was regenerated using 1.5 M KCl, 20 mM Tris-HCl pH 8.0, 1 % w/v CHAPS (100 µl min^{-1}, 1 min). $WIF\text{-}1_{Full\ length}$ - Wnt3a binding experiments in the presence of 2 mM $CaCl_2$ pH 8.0 or 2 mM EDTA pH 8.0 were performed in 150 mM NaCl, 20 mM Tris-HCl pH 8.0, 1 % w/v CHAPS running buffer (buffer A); $WIF\text{-}1_{WD\text{-}EGF\text{-}I}$ - Wnt3a binding experiments in the presence of 2 mM phosphocholine chloride calcium salt tetrahydrate (Sigma) were performed in buffer A or in 150 mM NaCl, 20 mM HEPES pH 7.5, 1 % w/v CHAPS running (buffer B). All experiments (including WIF-1 binding to GAGs, see below) were performed in triplicate (only $WIF\text{-}1_{WD\text{-}EGF\text{-}I}$ - Wnt3a binding experiment in the presence of phosphocholine chloride in buffer B was performed in duplicate). K_d values were calculated using BIAevaluation 3.0 program (Biacore Life Sciences) and a 1:1 Langmuir binding isotherm model.

SPR binding studies of WIF-1 and glycosaminoglycans. Heparin polymer (MW higher than 9000 g mol^{-1}, Iduron), heparan sulfate from pig mucosa (Iduron), chondroitin sulfate sodium salt from shark cartilage (Sigma), and chondroitin 4-sulfate

sodium salt (Fluka) were biotinylated with EZ-Link Biotin-LC-Hydrazide (Thermo Fisher Scientific) in aqueous 17 % v/v DMSO solution (36 h, 20 °C), then extensively dialyzed against water and SPR running buffer (120 mM NaCl, 10 mM HEPES pH 7.5, 0.05 % v/v Tween 20). Biotinylated GAGs were immobilized on the streptavidin-coated SPR sensor surface. For measurements of WIF-1 binding to immobilized GAGs, the same experimental settings as for WIF-1-Wnt3a were used. The sensor surface was regenerated using 1.5 M NaCl, 10 mM HEPES pH 7.5, 0.05 % v/v Tween 20.

SUPPLEMENTARY FIGURES

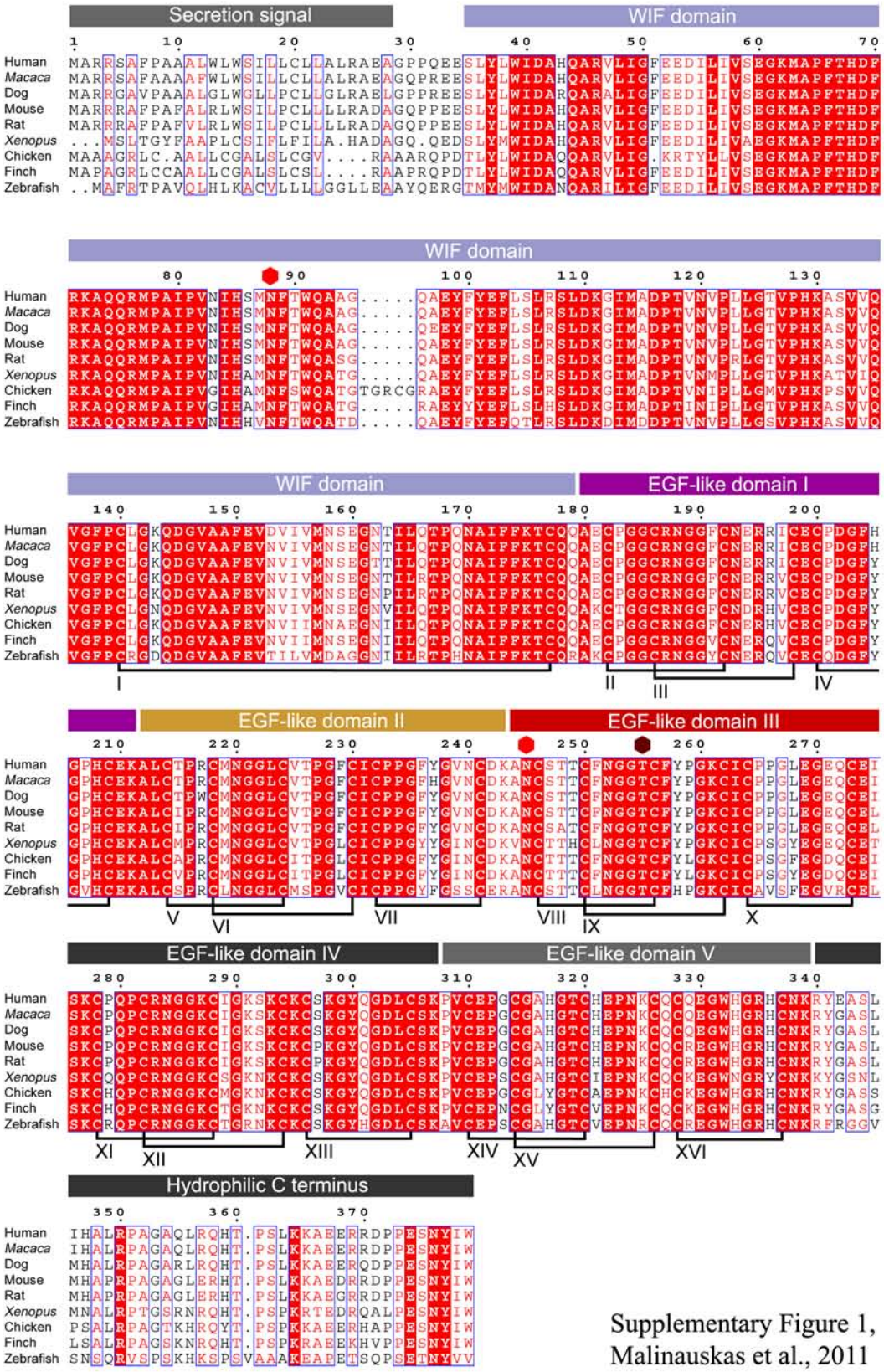

Supplementary Figure 1,
Malinauskas et al., 2011

Supplementary Figure 1 Amino acid sequence alignment of the vertebrate WIF-1 family members. Alignment of human (SwissProt identification accession number Q9Y5W5), *Macaca mulatta* (NCBI reference sequence XP_538269.2), dog (NCBI XP_538269.2), mouse (SwissProt Q9WUA1), rat (SwissProt Q6IN38), *Xenopus laevis* (SwissProt Q9W6F8), chicken (NCBI NP_001186536), zebra finch (*Taeniopygia guttata*, NCBI XP_002188540.1), zebrafish (SwissProt Q9W6F9) WIF-1, respectively. The sequences were aligned using MultAlin[16] (http://multalin.toulouse.inra.fr/) and formatted with ESPript[17] (http://espript.ibcp.fr/). Numbering corresponds to the full length human WIF-1. Evolutionarily conserved residues are shown in a red background. Disulfide bridges are indicated and marked with Roman numerals. The color scheme corresponds to that in **Fig. 4a**. Following WIF-$1_{\Delta C}$ crystal structure refinement, electron density corresponding to the N-linked N-acetylglucosamine could be seen at two glycosylation sites: Asn88 and Asn245 (marked by filled red hexagons). O-linked fucose could be seen at one glycosylation site, Thr255 (marked by filled brown hexagon).

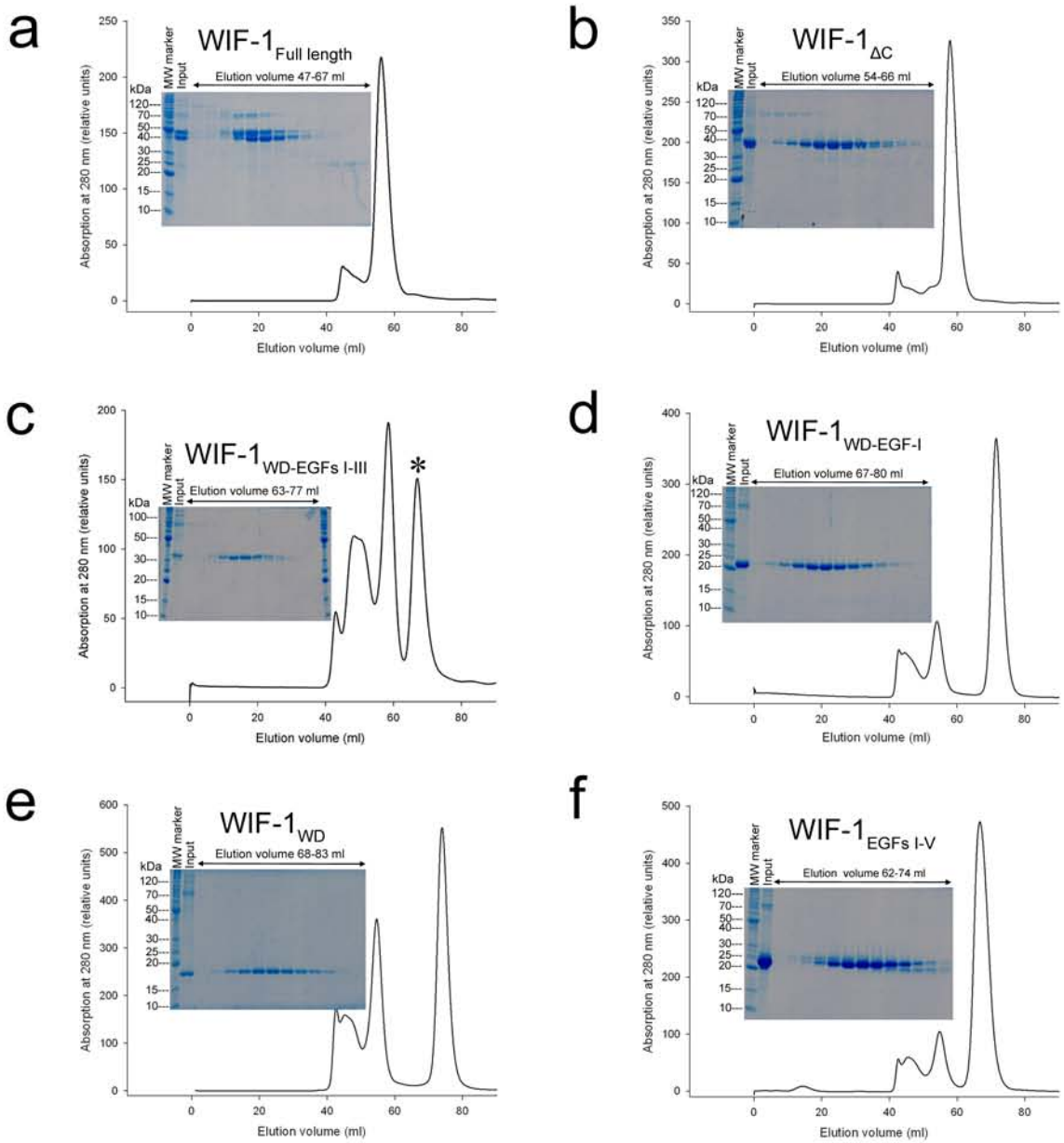

Supplementary Figure 2 Size-exclusion chromatography of WIF-1 constructs. Size-exclusion chromatography of WIF-1 constructs: (**a**) WIF-$1_{\text{Full length}}$, (**b**) WIF-$1_{\Delta C}$, (**c**) WIF-$1_{\text{WD-EGFs I-III}}$, (**d**) WIF-$1_{\text{WD-EGF-I}}$, (**e**) WIF-1_{WD}, and (**f**) WIF-$1_{\text{EGFs I-V}}$. Separation by size exclusion chromatography was performed using HiLoad 16/60 Superdex 75 column (GE Healthcare Life Sciences) at a flow speed of 0.8 ml min^{-1} in 20 mM Tris-HCl pH 8.0, 300 mM NaCl. Protein elution was monitored by absorbance at 280 nm (black curves). WIF-1 peak fractions were analyzed on reducing SDS-polyacrylamide (15 % w/v) gels (insets). WIF-$1_{\text{WD-EGFs I-III}}$ (residues 35–274) expresses at significantly lower levels (**c**). The expressed protein is present in the peak marked with an asterisk (*); three slightly longer WIF-$1_{\text{WD-EGFs I-III}}$ constructs (residues 35–275, 35–276, 35–277) were not secreted by HEK293T cells (data not shown). Molecular weight (MW) marker: BenchMark Protein Ladder, Invitrogen. Gels were stained with SimplyBlue SafeStain, Invitrogen.

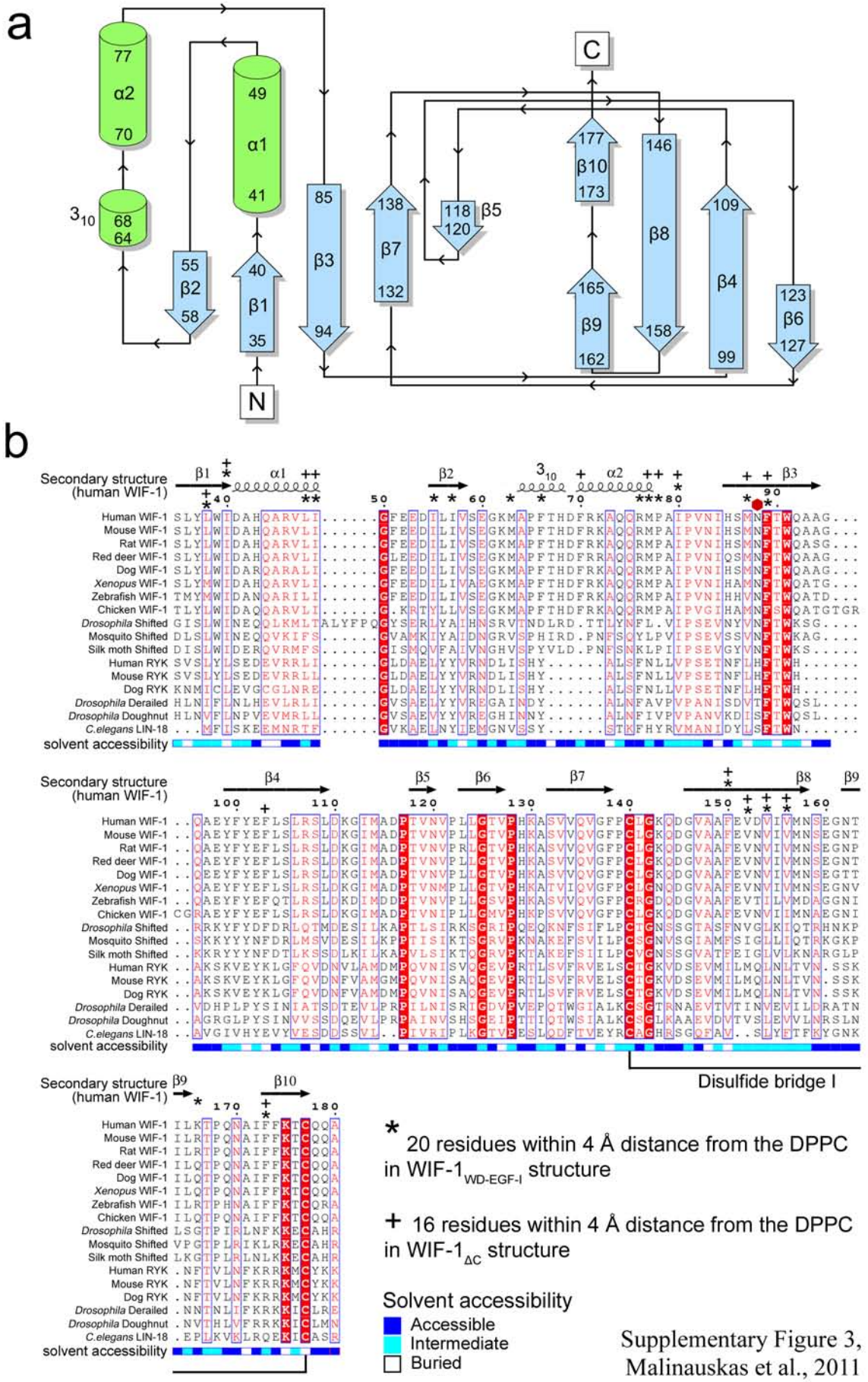

Supplementary Figure 3,
Malinauskas et al., 2011

Supplementary Figure 3 Topology diagram of the human WIF-1 WD and amino acid sequence alignment of the WDs. (**a**) Topology diagram of the human WIF-1 WD. α helices are shown as green cylinders, β strands are shown as light blue arrows. Amino acid sequence boundaries of each secondary structure element correspond to the full length human WIF-1 (including secretion signal). The topology diagram was generated using program PDBsum[18] (http://www.ebi.ac.uk/pdbsum/) for the WD of the WIF-$1_{WD\text{-}EGF\text{-}I}$ crystal structure and modified using program Inkscape (http://www.inkscape.org/). (**b**) Amino acid sequence alignment of the WIF domains. Alignments of human (residues 35–180, SwissProt identification accession number Q9Y5W5), mouse (residues 35–180, SwissProt Q9WUA1), rat (residues 35–180, SwissProt Q6IN38), red deer (*Cervus elaphus*, residues 3–148, UniProtKB/TrEMBL A6YLN5), dog (residues 35–180, National Center for Biotechnology Information, U.S. National Library of Medicine (NCBI) identification accession number XP_538269.2), *Xenopus laevis* (residues 30–175, Swiss-Prot Q9W6F8), zebrafish (residues 33–178, SwissProt Q9W6F9), chicken (residues 30–179, NCBI XP_416072.2) WIF domains of WIF-1 proteins, and WIF domains of *Drosophila* Shifted (residues 116–264, SwissProt Q9W3W5), African malaria mosquito Shifted (*Anopheles gambiae*, residues 46–189, XP_311028.4), silk moth Shifted (*Bombyx mori*, residues 38–180, NCBI NP_001040227.1), human RYK (residues 60–194, SwissProt P34925), mouse RYK (residues 47–181, SwissProt Q01887), dog RYK (residues 36–170, NCBI XP_534269.2), *Drosophila* Derailed (residues 21–158, SwissProt Q27324) and Doughnut (residues 46–183, SwissProt Q9V422), *Caenorhabditis elegans* Abnormal cell lineage protein 18 (residues 1–129, TrEMBL Q18041), respectively. The sequences were aligned using MultAlin[16] (http://multalin.toulouse.inra.fr/) and formatted with ESPript[17] (http://espript.ibcp.fr/). Numbering corresponds to the full length human WIF-1. Secondary structure assignments (calculated using program PDBsum[18] (http://www.ebi.ac.uk/pdbsum/)) for the WD of WIF-$1_{WD\text{-}EGF\text{-}I}$ crystal structure are displayed above the alignment and correspond to **Supplementary Fig. 3a**. Disulfide bridge I (between Cys140 and Cys177) and the solvent accessibilities (calculated with ESPript) of WIF-1 residues are presented below the alignments (blue, accessible; cyan, intermediate; white, buried). An N-linked N-acetylglucosamine is marked by a filled red hexagon above glycosylated Asn88. Twenty residues within 4 Å of the DPPC in the WIF-$1_{WD\text{-}EGF\text{-}I}$ structure are marked with an asterisk (*). Sixteen residues within 4 Å of the DPPC in the WIF-$1_{\Delta C}$ structure are marked with a plus sign (+).

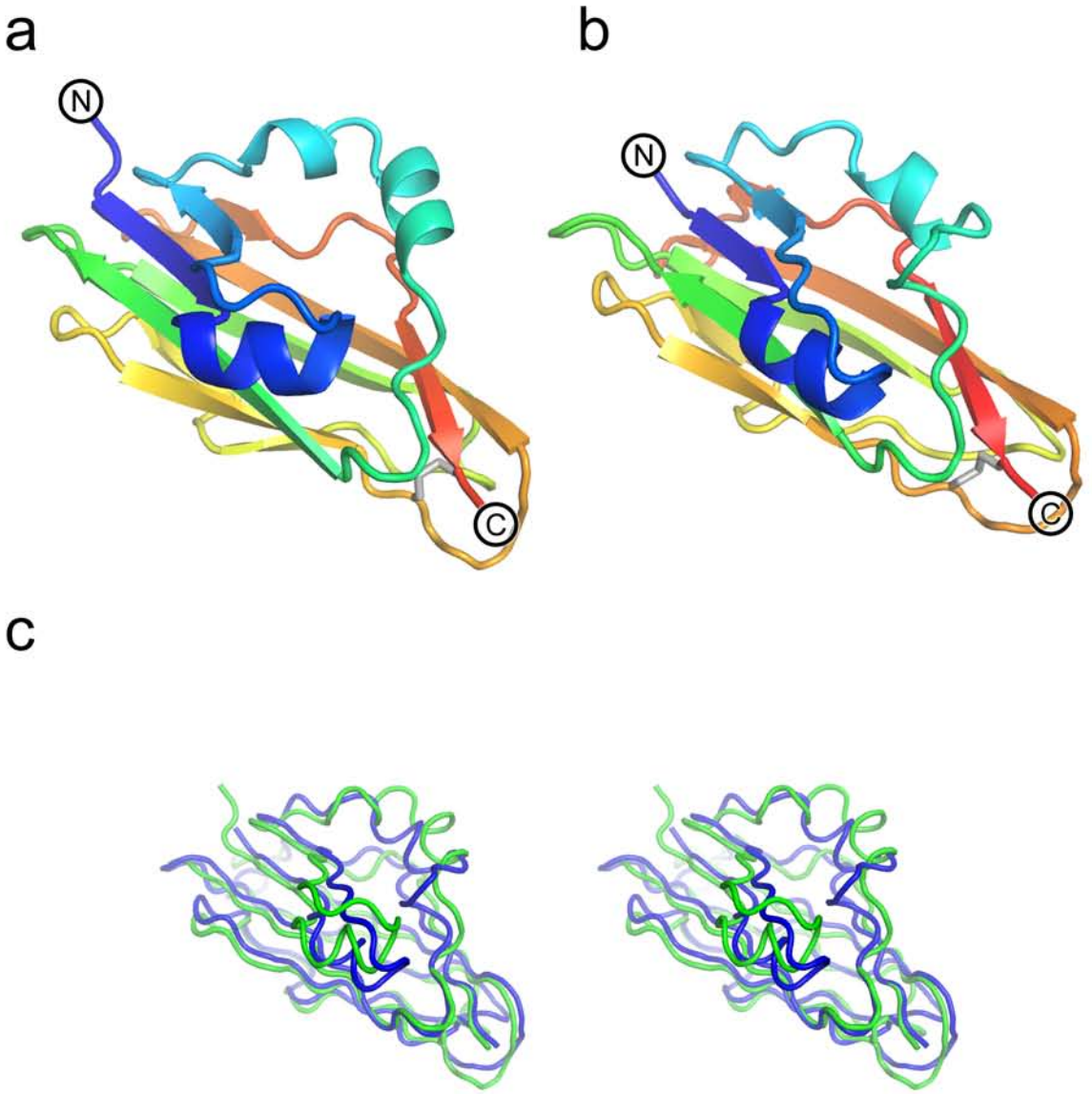

Supplementary Figure 4 Comparison of the human WIF-1 WD structures. Comparison of the WD structures solved by (**a**) X-ray crystallography and (**b**) solution NMR[5] (Protein Data Bank ID code 2D3J, model 1). The orientation of the WD is the same as in **Fig. 1b** (0° view). DPPC is not shown. (**c**) Superposition of **a** (green) and **b** (blue), stereo view.

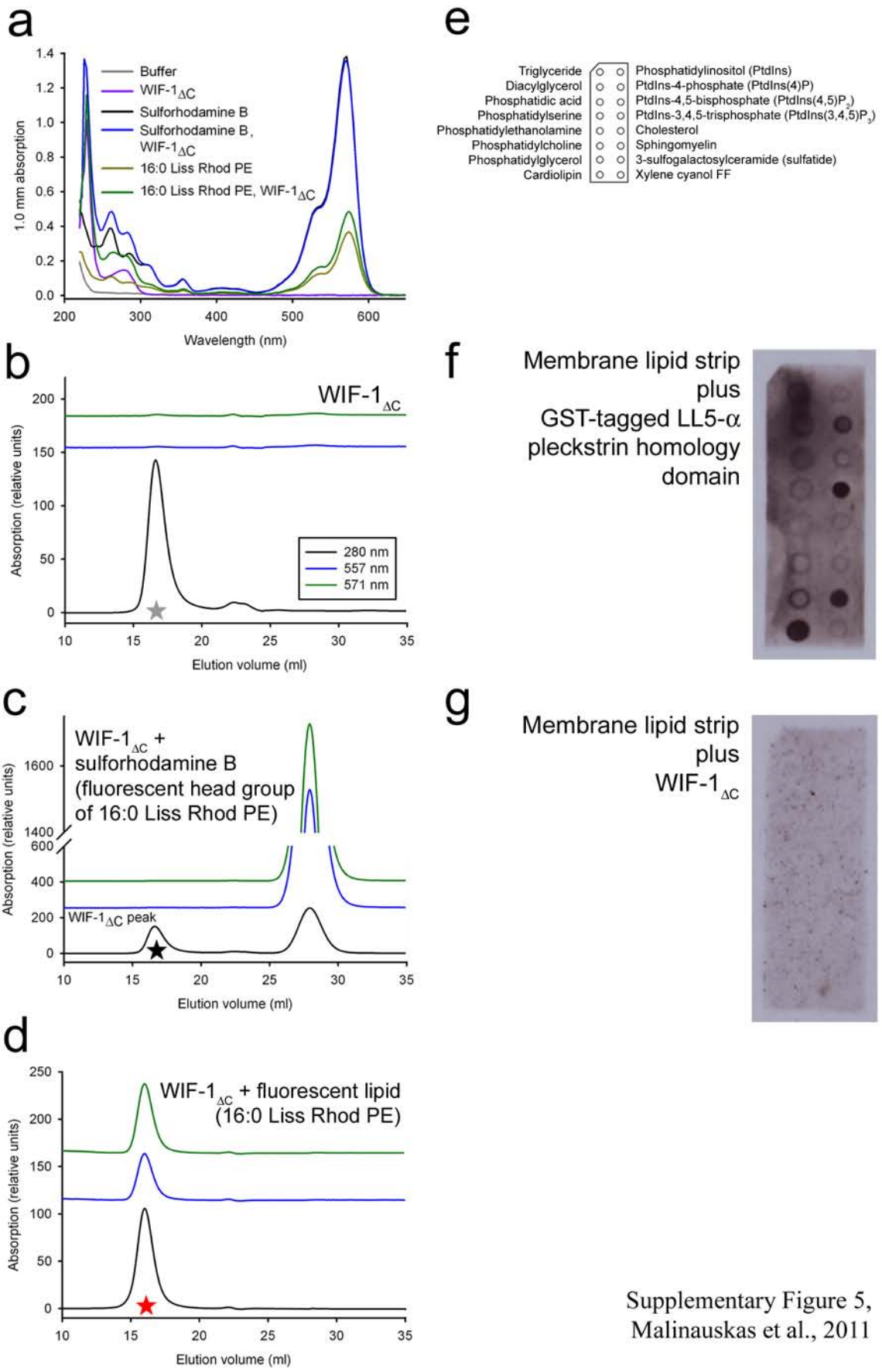

Supplementary Figure 5,
Malinauskas et al., 2011

Supplementary Figure 5 WIF-1 interactions with a fluorescent DPPC analogue and biologically abundant lipids. (**a**) Absorption spectra of solutions used in WIF-1-fluorescent molecule binding studies: buffer (PBS plus 1 % w/v CHAPS; grey curve), WIF-$1_{\Delta C}$ (50 μM, purple), sulforhodamine B (160 μM, black), sulforhodamine B (160 μM) plus WIF-$1_{\Delta C}$ (50 μM) (blue), 16:0 Liss Rhod PE (10 μl (1 mg ml^{-1} in $CHCl_3$) in 270 μl buffer; dark yellow), 16:0 Liss Rhod PE plus WIF-$1_{\Delta C}$ (50 μM) (10 μl (1 mg ml^{-1} in $CHCl_3$) in 270 μl buffer plus WIF-$1_{\Delta C}$; green). (**b**-**d**) Size-exclusion chromatography of the purified WIF-$1_{\Delta C}$ incubated: (**b**) without fluorescent molecules, (**c**) with sulforhodamine B (fluorescent head group of 16:0 Liss Rhod PE) and (**d**) with 16:0 Liss Rhod PE. Separation by size exclusion was performed using Superdex 200 10/300 column (GE Healthcare Life Sciences) at a flow speed of 0.4 ml min^{-1} in PBS at room temperature. Protein and fluorescent molecule elution was monitored by absorbance at 280, 557 and 571 nm (black, blue and green curves, respectively) simultaneously. Binding between WIF-$1_{\Delta C}$ and 16:0 Liss Rhod PE was confirmed by fluorescence (excitation at 535 nm, emission at 595 nm) intensity measurements: intensity of WIF-$1_{\Delta C}$ peak fractions containing 16:0 Liss Rhod PE (indicated with a red star in **d**) was hundred fold (100 %) higher than WIF-$1_{\Delta C}$ alone (0.7 %; indicated with a grey star in **b**) or WIF-$1_{\Delta C}$ incubated with sulforhodamine B (0.4 %; indicated with a black star in **c**). (**e**) Details of the 15 commercially available, pre-spotted lipids on the hydrophobic membrane strip (Echelon Biosciences Inc.). (**f**) Western blot of the membrane strip (**e**) after incubation with a glutathione S-transferase (GST)-tagged LL5-α pleckstrin homology domain (MultiPIP Grip, Echelon Biosciences) and anti-GST horseradish peroxidase (HRP) conjugate (GE Healthcare Life Sciences) as a positive control experiment. HRP was detected by chemiluminescence using the Amersham ECL detection kit (GE Healthcare Life Sciences). Dark round spots on the strip indicate protein-lipid interactions. (**g**) Western blot of the membrane strip (**e**) after incubation with a His-tagged WIF-$1_{\Delta C}$, anti-PentaHis monoclonal primary antibody (Qiagen) and goat anti-mouse IgG HRP conjugate (Sigma).

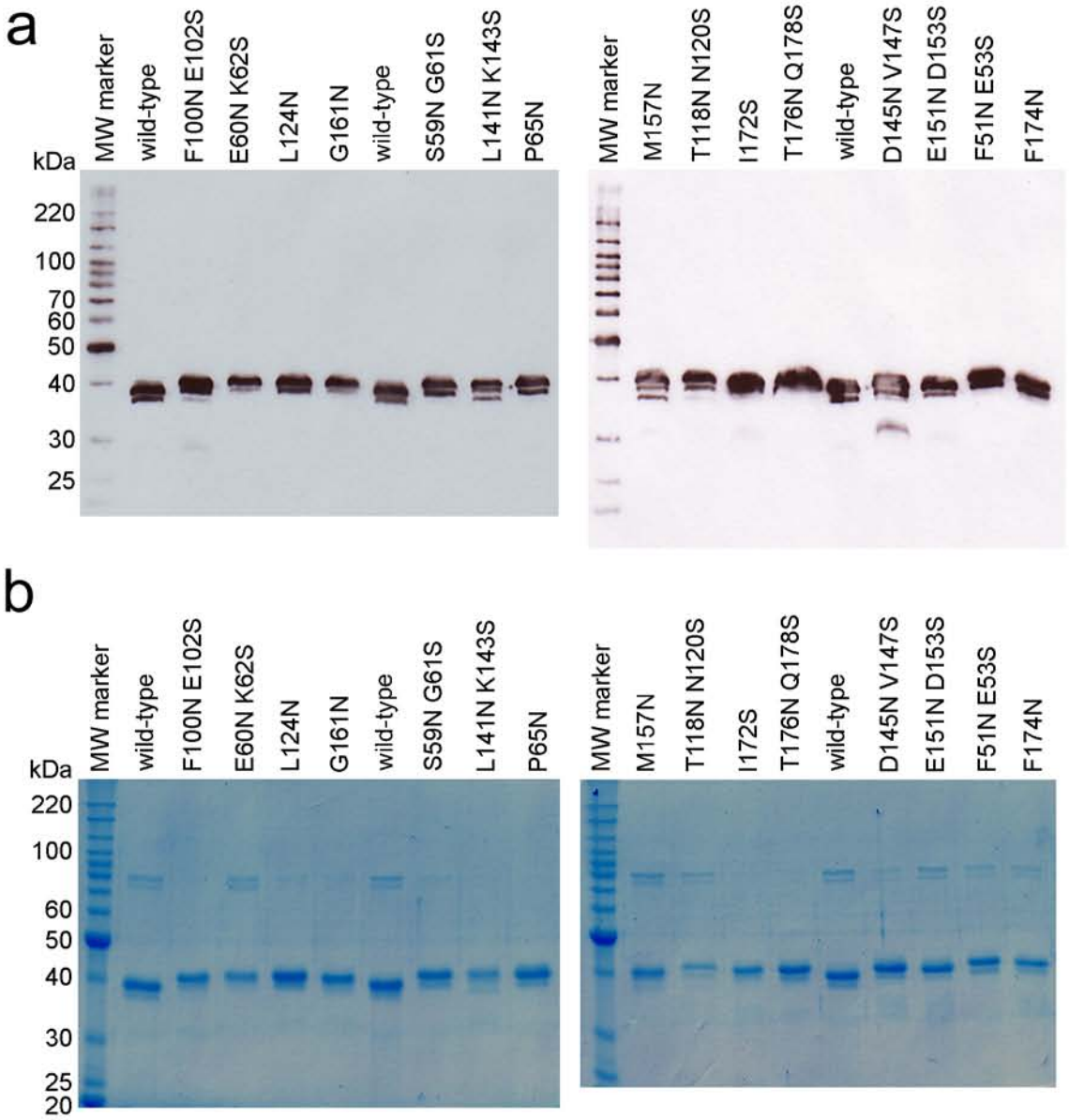

Supplementary Figure 6 (**a**) Western blot and (**b**) SDS-polyacrylamide gel electrophoretic analysis of the purified WIF-$1_{\Delta C}$ constructs. Mutations (indicated above each lane) introduce an Asn-linked glycosylation site and increase molecular weight (MW) of WIF-$1_{\Delta C}$. Reducing SDS-polyacrylamide (12 % w/v) gels were used. Western blots were probed with anti-PentaHis monoclonal primary antibody (Qiagen) and goat anti-mouse IgG horseradish peroxidase (HRP) conjugate (Sigma). HRP was detected by chemiluminescence using the Amersham ECL detection kit (GE Healthcare Life Sciences) in **a**. Gels were stained with SimplyBlue SafeStain, Invitrogen, in **b**. MW marker: BenchMark Protein Ladder, Invitrogen.

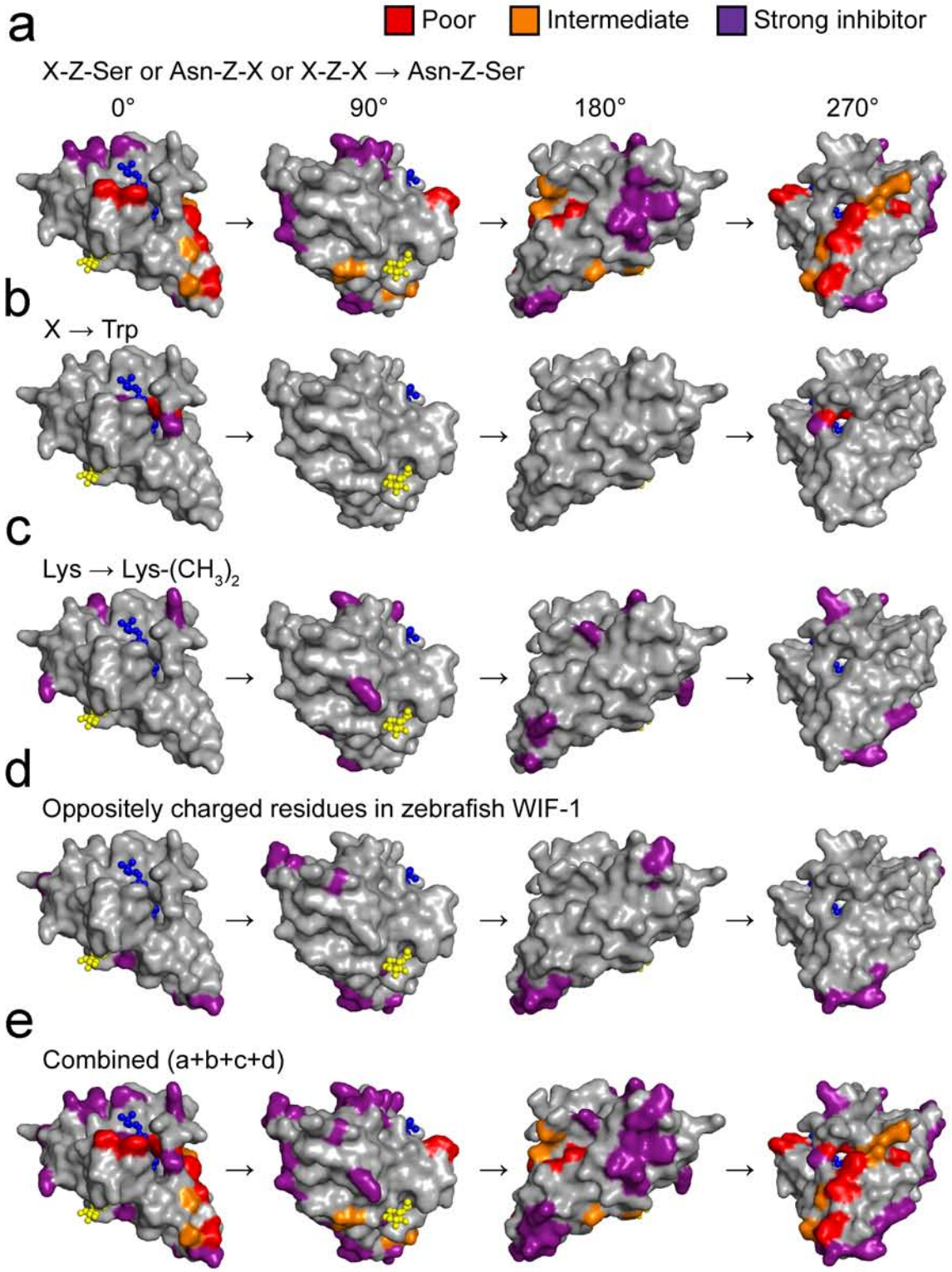

Supplementary Figure 7,
Malinauskas et al., 2011

Supplementary Figure 7 Residues tested in the cellular assay for Wnt3a signaling inhibition mapped on the WD surface. (**a**) The locations of introduced glycosylation sites on the WD surface. Orientation of the WD is the same in the 0° view as in **Fig. 1b** (left panel). The wild-type GlcNAc moiety on Asn88 is shown as yellow spheres. Residues for which the putative glycosylation site generating mutations resulted in poor inhibition of Wnt3a signaling are colored in red (Phe174, Phe51, Glu53, Glu151, Asp153, Asp145, and Val147), residues that were mutated and resulted in intermediate (Thr176, Gln178, Ile172, Thr118, and Asn120) and strong (Met157, Phe65, Leu141, Lys143, Ser59, Gly61, Gly161, Leu124, Glu60, Lys62, Phe100, and Glu102) inhibition of Wnt3a signaling are colored in orange and purple, respectively. Color coding corresponds to **Fig. 3a**. (**b**) The locations of mutations which introduced tryptophans: Met77 (red), Ile55 (purple), and Pro78 (purple). (**c**) The locations of lysines (purple). (**d**) The locations of human WIF-1 residues for which the equivalent residues in zebrafish WIF-1 differ in electrostatic charge (purple, human WIF-1 residue and number/corresponding zebrafish residue): Ser86/His, Gly95/Asp, Gly112/Asp, Ala115/Asp, Leu141/Arg, Lys143/Asp, Asn158/Asp, Gln179/Arg, and Glu160/Gly. (**e**) The combined information from **a** to **d** indicates a potential WD surface that is (orange and red) or is not (purple) recognized by human Wnt3a.

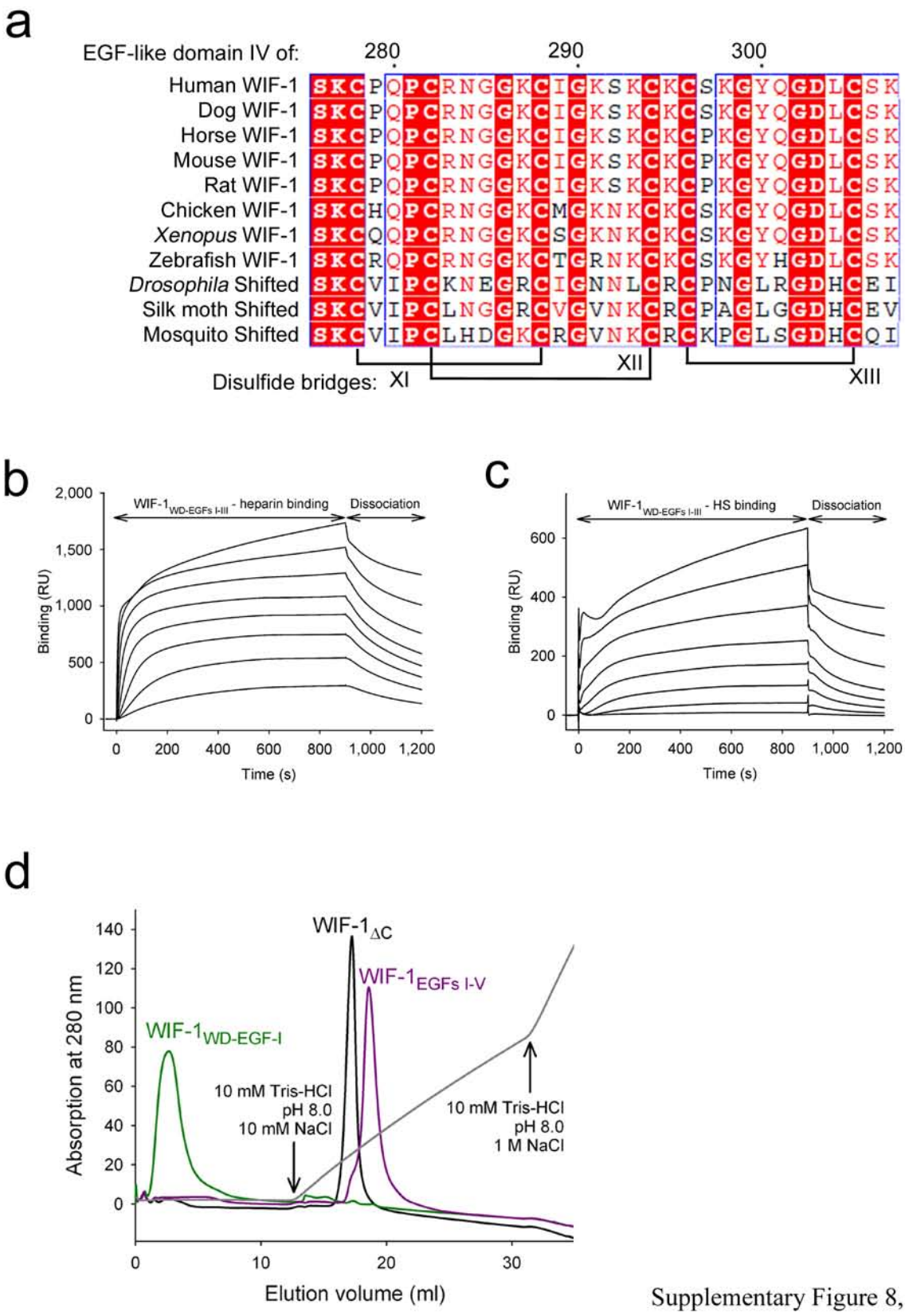

Supplementary Figure 8,
Malinauskas et al., 2011

Supplementary Figure 8 Heparin- and heparan sulfate-binding properties of human WIF-1. (**a**) Amino acid sequence alignment of the WIF-1 EGF-like domain IV for mammals, chicken, *Xenopus* and zebrafish plus of the equivalent domain from sequences for the insect protein Shifted. Evolutionarily conserved residues are shown in a red background. Three disulfide bridges are indicated and marked with Roman numerals. Numbering corresponds to the full length human WIF-1 (including secretion signal), SwissProt identification accession number Q9Y5W5. (**b** and **c**) SPR binding sensorgrams of WIF-$1_{\text{WD-EGFs I-III}}$ to glycosaminoglycans. SPR binding sensorgrams in which a concentration series (15.0 nM–1.92 μM, two-fold dilutions) of WIF-$1_{\text{WD-EGFs I-III}}$ was injected over immobilized heparin (**b**) or heparan sulfate (**c**). These SPR sensorgrams could not be fitted to conventional 1:1 equilibrium or kinetic interaction models using BIAevaluation (Biacore Life Sciences) software, possibly indicating some contribution to binding from disruption of the terminal EGF-like domain III structure, consistent with the observed sensitivity to the exact C terminal truncation point (**Supplementary Fig. 2c**). (**d**) Binding of WIF-1 constructs to heparin column. Three constructs of WIF-1 (WIF-$1_{\text{WD-EGF-I}}$ (green), WIF-$1_{\text{EGFs I-V}}$ (purple), and WIF-$1_{\Delta C}$ (black)) were dialyzed against 10 mM Tris-HCl pH 8.0, 10 mM NaCl and loaded onto a pre-equilibrated 5 ml heparin column (HiTrap Heparin HP, GE Healthcare Life Sciences). Protein elution was followed by absorption at 280 nm. The elution gradient is represented by the grey curve. Arrows indicate the gradient range of NaCl (10–1000 mM). The WIF-$1_{\text{WD-EGF-I}}$ construct did not bind to the column and was eluted with the binding buffer (elution volume 1–5 ml). The WIF-$1_{\text{EGFs I-V}}$ and WIF-$1_{\Delta C}$ constructs were eluted with higher NaCl concentration (300 mM and 250 mM, respectively) indicating binding to the heparin.

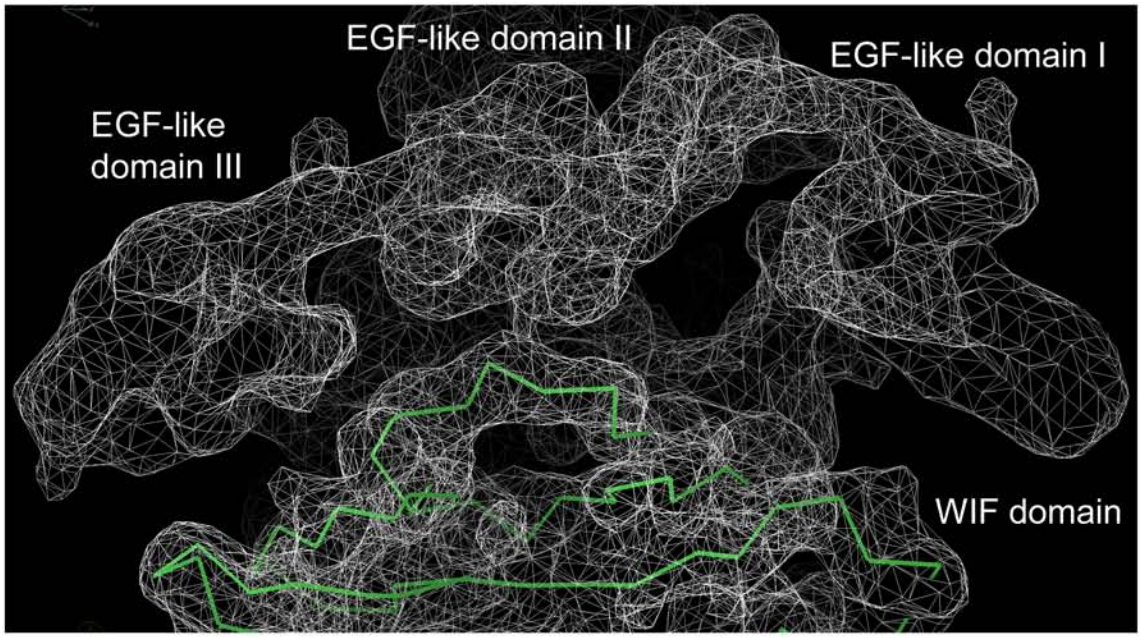

Supplementary Figure 9 Initial WIF-$1_{\Delta C}$ $2F_o$-F_c electron density map. Initial WIF-$1_{\Delta C}$ $2F_o$-F_c electron density map calculated after molecular replacement using the high resolution crystallographic structure of the WD as a search model and subsequent phase improvement by solvent flattening (crystals of WIF-$1_{\Delta C}$ contain 82 % solvent) and histogram matching using program Parrot[12]. Electron density is contoured at 1 σ using program Coot[7]. Cα backbone of the WD is shown in green. Electron density corresponding to the EGF-like domains I to III is apparent.

SUPPLEMENTARY REFERENCES

1. Walter, T.S., Diprose, J.M., Mayo, C.J., Siebold, C., Pickford, M.G., Carter, L., Sutton, G.C., Berrow, N.S., Brown, J., Berry, I.M., Stewart-Jones, G.B., Grimes, J.M., Stammers, D.K., Esnouf, R.M., Jones, E.Y., Owens, R.J., Stuart, D.I., and Harlos, K. (2005) A procedure for setting up high-throughput nanolitre crystallization experiments. Crystallization workflow for initial screening, automated storage, imaging and optimization. Acta Crystallogr. D Biol. Crystallogr. 61, 651-657.
2. Otwinowski, Z. and Minor, W. (1997) Processing of X-ray diffraction data collected in oscillation mode. Methods Enzymol. 276, 307-326.
3. Kabsch, W. (2010) Integration, scaling, space-group assignment and post-refinement. Acta Crystallogr. D Biol. Crystallogr. 66, 133-144.
4. Evans, P. (2006) Scaling and assessment of data quality. Acta Crystallogr. D Biol. Crystallogr. 62, 72-82.
5. Liepinsh, E., Bányai, L., Patthy, L., and Otting, G. (2006) NMR structure of the WIF domain of the human Wnt-inhibitory factor-1. J. Mol. Biol. 357, 942-950.
6. McCoy, A.J., Grosse-Kunstleve, R.W., Storoni, L.C., and Read, R.J. (2005) Likelihood-enhanced fast translation functions. Acta Crystallogr. D Biol. Crystallogr. 61, 458-464.
7. Emsley, P., Lohkamp, B., Scott, W.G., and Cowtan, K. (2010) Features and development of Coot. Acta Crystallogr. D Biol. Crystallogr. 66, 486-501.
8. Blanc, E., Roversi, P., Vonrhein, C., Flensburg, C., Lea, S.M., and Bricogne, G. (2004) Refinement of severely incomplete structures with maximum likelihood in BUSTER-TNT. Acta Crystallogr. D Biol. Crystallogr. 60, 2210-2221.
9. Adams, P.D., Afonine, P.V., Bunkóczi, G., Chen, V.B., Davis, I.W., Echols, N., Headd, J.J., Hung, L.W., Kapral, G.J., Grosse-Kunstleve, R.W., McCoy, A.J., Moriarty, N.W., Oeffner, R., Read, R.J., Richardson, D.C., Richardson, J.S., Terwilliger, T.C., and Zwart, P.H. (2010)

PHENIX: a comprehensive Python-based system for macromolecular structure solution. Acta Crystallogr. D Biol. Crystallogr. 66, 213-221.

10. Hsin, K., Sheng, Y., Harding, M.M., Taylor, P., and Walkinshaw, M.D. (2008) MESPEUS: a database of the geometry of metal sites in proteins. J. Appl. Cryst. 41, 963-968.
11. Terwilliger, T.C., Grosse-Kunstleve, R.W., Afonine, P.V., Moriarty, N.W., Adams, P.D., Read, R.J., Zwart, P.H., and Hung, L.W. (2008) Iterative-build OMIT maps: map improvement by iterative model building and refinement without model bias. Acta Crystallogr. D Biol. Crystallogr. 64, 515-524.
12. Zhang, K.Y., Cowtan, K., and Main, P. (1997) Combining constraints for electron-density modification. Methods Enzymol. 277, 53-64.
13. Davis, I.W., Leaver-Fay, A., Chen, V.B., Block, J.N., Kapral, G.J., Wang, X., Murray, L.W., Arendall, W.B. 3rd, Snoeyink, J., Richardson, J.S., Richardson, D.C. (2007) MolProbity: all-atom contacts and structure validation for proteins and nucleic acids. Nucleic Acids Res. 35, W375-383.
14. Schiller, J., Arnhold, J., Benard, S., Müller, M., Reichl, S., and Arnold, K. (1999) Lipid analysis by matrix-assisted laser desorption and ionization mass spectrometry: A methodological approach. Anal Biochem. 267, 46-56.
15. DasGupta, R., Kaykas, A., Moon, R.T., and Perrimon, N. (2005) Functional genomic analysis of the Wnt-wingless signaling pathway. Science. 308, 826-833.
16. Corpet, F. (1988) Multiple sequence alignment with hierarchical clustering. Nucleic Acids Res. 16, 10881-10890.
17. Gouet, P., Courcelle, E., Stuart, D.I., and Métoz, F. (1999) ESPript: analysis of multiple sequence alignments in PostScript. Bioinformatics 15, 305-308.
18. Laskowski, R.A. (2009) PDBsum new things. Nucleic Acids Res. 37 (Database issue), D355-359.